Subgrid informed neural networks for high-resolution flood mapping

Herath, Herath Mudiyanselage Viraj Vidura; Marshall, Lucy; Saha, Abhishek; Rasnayaka, Sanka; Seneviratne, Sachith

DOI
10.1016/j.jhydrol.2025.133329

Publication date
2025

Document Version
Final published version

Published in
Journal of Hydrology

Citation (APA)
Herath, H. M. V. V., Marshall, L., Saha, A., Rasnayaka, S., & Seneviratne, S. (2025). Subgrid informed neural networks for high-resolution flood mapping. *Journal of Hydrology*, *660*, Article 133329. https://doi.org/10.1016/j.jhydrol.2025.133329

Journal of Hydrology 660 (2025) 133329

Contents lists available at ScienceDirect

Journal of Hydrology

journal homepage: www.elsevier.com/locate/jhydrol

Research papers

Subgrid informed neural networks for high-resolution flood mapping

Herath Mudiyanselage Viraj Vidura Herath [a,*], Lucy Marshall [a,b], Abhishek Saha [c,d], Sanka Rasnayaka [e], Sachith Seneviratne [f,g]

[a] Faculty of Science and Engineering, Macquarie University, Sydney, New South Wales, Australia
[b] Faculty of Engineering, The University of Sydney, Sydney, New South Wales, Australia
[c] Delft Institute of Applied Mathematics, Delft University of Technology, Delft, The Netherlands
[d] Hydroinformatics Institute, Singapore
[e] Department of Computer Science, School of Computing, National University of Singapore, Singapore
[f] Transport, Health and Urban Systems Research Lab, Melbourne School of Design, The University of Melbourne, Melbourne, Victoria, Australia
[g] Faculty of Engineering and Information Technology, The University of Melbourne, Melbourne, Victoria, Australia

ARTICLE INFO

This manuscript was handled by Andras Bardossy, Editor-in-Chief, with the assistance of Ankit Agarwal, Associate Editor.

Keywords:
Flood mapping
U-net
Physics-informed machine learning
Hybrid models
Subgrid
Super-resolution

ABSTRACT

Physics-based hydrodynamic models are essential for accurate flood prediction but are computationally expensive, limiting their applicability for real-time forecasting and probabilistic analyses. Conversely, pure machine learning (ML) models offer both computational efficiency and accuracy but often lack interpretability. To address this gap, we propose SGUnet, a physics-informed ML model and a hybrid theory-guided data science approach, for rapid, high-resolution flood mapping. It utilizes a neural network with U-Net architecture and integrates subgrid-based coarse-grid hydrodynamic model predictions as initial estimates, upskilling them to achieve fine-grid model accuracy. Unlike traditional hydrodynamic models, the subgrid method embeds fine-scale topographic details within coarse-grid cells, enhancing both computational efficiency and predictive accuracy.

SGUnet processes flood depth raster patches (512 × 512 pixels) and corresponding digital elevation models as inputs. It functions as a deep learning-based corrector, refining flood predictions from numerical simulators. Trained through supervised learning, SGUnet learns to correct deviations in coarse-grid predictions using fine-grid model outputs as target values. The model is evaluated across three large Australian watersheds—Wollombi, Chowilla, and Burnett River—using HEC-RAS flood simulations with subgrid formulation. SGUnet reduces root mean squared error by a factor of 4.5–5.3 compared to coarse-grid models, achieves a critical success index exceeding 0.9 for flood extent mapping, and delivers a 50x speed-up over fine-grid hydrodynamic models. Furthermore, SGUnet outperforms a state-of-the-art ML-based upskilling model in depth and extent predictions. By effectively correcting flood artifacts from coarse-grid models, SGUnet achieves near fine-grid accuracy with significantly reduced computational cost, demonstrating its potential for real-time flood risk assessment.

1. Introduction

According to records (World Health Organisation, 2024), floods are the most frequent natural disaster worldwide and, in Australia, they are also the most costly. The recent floods in 2022 caused AUD 6.3 billion in insured damages (The Insurance Council of Australia, 2024). However, floods are also among the most manageable natural disasters.

Hydrodynamic modeling is a powerful tool for understanding and managing flood risks, simulating water movement using physical laws such as the Navier–Stokes equations and shallow water equations (SWE). Although high-resolution models offer accuracy, their high computational cost makes them impractical for large-scale operational flood modeling and probabilistic flood design, where numerous simulations are required (Fraehr et al., 2024).

Efforts to improve computational efficiency of hydrodynamic models include CPU/GPU-based parallel computations (Rak et al., 2024), the adoption of advanced modeling techniques such as subgrid sampling (Stelling, 2022), and the implementation of faster solver schemes (Buwalda et al., 2023). Numerical advances in SWE solvers, particularly through the use of subgrid methods, have significantly accelerated simulations of pluvial and coastal flooding utilizing high-resolution topographic data (Stelling, 2022; Casulli, 2019). The subgrid approach facilitates coarse-grid simulations by assuming uniform water levels

* Corresponding author.
E-mail address: viraj.vidura@mq.edu.au (H.M.V.V. Herath).

https://doi.org/10.1016/j.jhydrol.2025.133329
Received 6 November 2024; Received in revised form 17 March 2025; Accepted 14 April 2025
Available online 28 April 2025

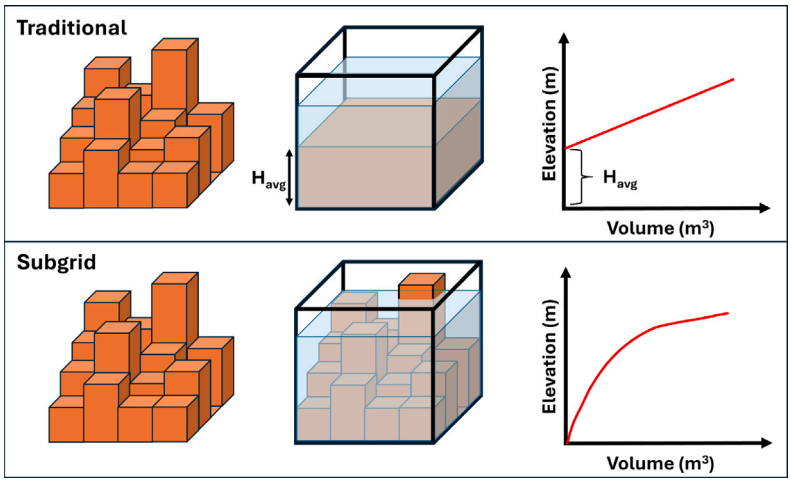

Fig. 1. An example representation of bathymetry within a computational cell of a traditional model vs subgrid-based model.

within each coarse grid cell while allowing water depths to vary in response to microtopographic changes. This results in non-linear variations of volume within the computational coarse grids relative to water levels (Fig. 1), thereby providing accurate representations of flow processes in complex geometries compared to simulations without the subgrid formulation (Casulli and Stelling, 2011).

Despite its advantages, the subgrid model requires simplifications of the momentum balance within the coarse grid, as it relies on volume-averaged velocities and integral friction forces (Kennedy et al., 2019). These simplifications can introduce inaccuracies in flow patterns compared to fine-grid simulations, underscoring the need for grid convergence tests to verify model performance. Efforts to rectify flow characteristics have included the application of random forest-based machine learning (ML) methods (Ye et al., 2021). However, when the grids are excessively coarse and partially wet, the flow connectivities within subgrid cells may be misrepresented, leading to artificial flow-blocking effects. In scenarios where flow barriers, such as levees, must be accurately represented, it is essential to explicitly resolve fine grid topography to ensure proper flow blockage. To address these challenges, deterministic algorithms have been proposed (Casulli, 2019; Begmohammadi et al., 2021), but subgrid methods remain an active area of research.

Surrogate models provide a computationally efficient alternative to numerical hydrodynamic models by replicating their outputs using statistical or data-driven approaches. In flood mapping, they directly convert raw input data into flood depth or inundation predictions (Löwe et al., 2021; Zhou et al., 2021).

ML models, including deep learning (DL) models—a subset of surrogate models—are increasingly used in flood mapping for tasks such as susceptibility, inundation, and hazard mapping (Bentivoglio et al., 2022). Although pure data science models are highly computationally efficient, they often suffer from a lack of interpretability (black-box models) and low generalizability (overfitting). Model explainability is essential, as it improves understanding of the results, supports diverse operational needs, and enables evaluation of the model for potential inaccuracies when applied to new conditions.

Physics-informed machine learning (PIML), or theory-guided data science (TGDS) (Karpatne et al., 2017), addresses the limitations of purely data-driven models by incorporating scientific knowledge into learning algorithms to govern them. Hybrid TGDS models, which combine theory-based and data-driven approaches, are popular for their conceptual simplicity. In these models, part of the problem is solved using a theory-based model and the rest through a data science model (Karpatne et al., 2017). Additionally, interpretable physics informed neural networks (Ranasinghe et al., 2024) offer potential solutions to extracting the representation of the physical system (including differential equations) learned by such models.

Successful hybrid TGDS model applications can be found in many water resources applications, such as hydrological model building (Chadalawada et al., 2020; Herath et al., 2021a), rainfall runoff modeling (Herath et al., 2021b; Kapoor et al., 2023), and flood mapping (Fraehr et al., 2023). A complete overview on hybrid ML models in flood prediction is provided in Zuhairi et al. (2022). In flood modeling, hybrid models aim to combine the computational efficiency of data driven models with the accuracy, generalizability, and explainability of theory-based models. In a recent study (Fraehr et al., 2023), a Gaussian process-based hybrid model called low-fidelity, spatial analysis, and Gaussian process learning (LSG) model was introduced to upskill coarse grid hydrodynamic model results. The LSG model was benchmarked against several other surrogate models in Fraehr et al. (2024), where it was found to be more accurate for flood mapping compared to purely ML-based surrogate models. Other statistical approaches (Fraehr et al., 2023; Bryant et al., 2024; Carreau and Guinot, 2021) have been developed to enhance (upskill) coarse grid hydrodynamic model outputs to match high-resolution model results (a process known as super-resolution). Although purely ML-based surrogate models are more computationally efficient since they do not require numerical model runs at all, super-resolution models seem to achieve greater accuracy in high-resolution flood mapping (Fraehr et al., 2024).

In recent years, U-Net based super-resolution models have demonstrated success in upscaling coarse grid flooding simulations driven by rainfall in mountainous (He et al., 2023) and coastal tidal areas (Yin et al., 2024). However, this approach has yet to be tested in flow-rate-dominant domains or large-scale catchments. Additionally, U-Net DL models have proven effective as surrogate models for hydraulic models (Shao et al., 2024). These models utilize fine-scale geomorphological features to enhance flood depth and flood velocities (He et al., 2023). To cover large catchment areas, researchers have successfully trained U-Net on overlapping patches (Shao et al., 2024).

Another computationally efficient alternative to high-resolution numerical flood models, particularly in data-scarce regions, has been introduced and tested in flood-prone basins in Iran (Solaimani et al., 2023, 2024; Darvishi, 2025). These studies explore hybrid GIS-based and multi-criteria decision analysis approaches for flood hazard mapping, integrating spatial analysis, expert-driven decision models, and remote sensing data to assess flood risks across large areas. Unlike dynamic flood extent modeling, this methodology focuses on static flood hazard mapping based on spatial risk factors.

A coarse grid model with subgrid method operates significantly faster than a fine grid high-resolution model for the same study area, due to fewer computational cells and the ability to use larger computational time-steps. Despite these differences, the results of coarse grid

models are largely correlated with those of fine grid high-resolution models.

Building upon these advancements, this study introduces a novel hybrid TGDS U-Net model named SGUnet, designed for computationally efficient high-resolution flood mapping. We present a predictor–corrector formulation where initially, a subgrid hydrodynamic model is simulated with coarse grid configuration and its output is fed into a U-Net deep neural network. The U-Net enhances and corrects the initial flood depth estimates from the coarse grid model through a correction process, aligning them with the high-resolution fine grid flood model outputs. This approach achieves a balance between total computational speed – both during training and inference – and accuracy by leveraging the benefits of both numerical advancements such as subgrid and neural network architectures such as U-Net.

Compared to the flood mapping approaches discussed above, the SGUnet model offers several distinct advantages. Unlike methods that predict at fine grid mesh resolutions, SGUnet directly estimates flood depths at digital elevation model (DEM) resolution, eliminating the need for additional post-processing in flood mapping. Unlike previous U-Net-based super-resolution models that rely on interpolation to align resolutions, SGUnet directly incorporates high-resolution subgrid flood maps and DEMs from diverse catchments, simplifying data preparation and model training. Moreover, while purely ML-based approaches often lack interpretability, SGUnet is primarily driven by physics-based initial estimates from a coarse grid hydrodynamic model, enhancing its reliability and reducing overfitting. Unlike static flood hazard mapping techniques, SGUnet captures the full dynamic evolution of flood events. Additionally, a unique feature of SGUnet is its flexibility—it can generate a complete flood map for an entire basin or focus on specific local areas of interest, making it adaptable to different flood mapping needs.

The rest of the paper is organized as follows: Section 2 describes the workflow of the proposed SGUnet model. Section 3 discusses the application of the SGUnet model to three Australian watersheds, including a benchmark study. Finally, Section 4 outlines future research directions and presents the conclusions of the current study.

2. Material and methods

2.1. SGUnet model

The SGUnet model employs a U-Net-based ML architecture to enhance coarse-grid hydrodynamic flood maps. Each input sample for the model includes a flood depth raster image and the corresponding DEM image. Additionally, other spatial explanatory variables, such as slope, aspect, curvature, and flow accumulation, can be included and concatenated with the flood depth raster images. This approach allows SGUnet to integrate more hydrological insights into the process of refining coarse-grid simulations to closely align with fine-grid outputs.

U-Net is a type of convolutional neural network (CNN) which was originally developed for biomedical image segmentation in Ronneberger et al. (2015). U-Net is named for its characteristic U-shape, which arises from its symmetric encoder–decoder structure. Since its invention in 2015, U-Net has been widely used in various computer vision applications (Thisanke et al., 2023). In flood mapping, U-Net-based networks have been employed for tasks such as flood inundation mapping (Jamali et al., 2024), urban flood prediction (Löwe et al., 2021; Shao et al., 2024), coastal and riverine flood mapping (El baida et al., 2024), flash flood detection (Tuyen et al., 2021), post-disaster damage assessment (Madake et al., 2024), super-resolution (He et al., 2023; Yin et al., 2024), and uncertainty quantification (Li et al., 2024).

A U-Net requires both its input and output images to have the same resolution and be structured as arrays. However, most modern hydrodynamic models use unstructured computational meshes due to their flexibility in mesh generation. Additionally, fine-grid simulations, coarse-grid simulations, and spatial explanatory variables like DEM often exist at different resolutions. Typically, spatial explanatory variables have the highest resolution, when compared to the computational grids. In previous flood mapping super-resolution applications (Fraehr et al., 2023; He et al., 2023; Yin et al., 2024), different interpolation techniques were used to align different resolutions with that of the high-resolution model simulations. However, resampling values from high-resolution images like DEMs to a much coarser computational grid tend to lose the finer details that the high-resolution data can provide.

In contrast, the SGUnet framework converts both coarse and fine grid simulations into DEM resolution using a simpler approach based on subgrid topography. Water level values simulated by the hydrodynamic model at mesh resolution are transformed into water depth values at DEM resolution using subgrid topography. Once mapped to the DEM resolution, these simulations become structured arrays, with exactly same dimensions as the DEM itself. This process allows U-Nets to work with both structured and unstructured mesh simulations. Moreover, the conversion inherently integrates high-resolution topographic details while aligning different resolutions, simplifying the ML-based upscaling process.

2.1.1. Model architecture

The specific U-Net architecture used in the SGUnet model is shown in Fig. 2. It is based on the original U-Net architecture described in Ronneberger et al. (2015), but enhanced with attention blocks and conditioned on external data (e.g. DEM). The ML code for the SGUnet model is written in Python programming language (Python Software Foundation, 2024) using the PyTorch library (Paszke et al., 2019).

The left half of the network, known as the encoder (or contracting path), progressively reduces the spatial dimensions while capturing high-level features through a series of convolutional layers followed by pooling operations. The network accepts input in the form of a 512 × 512 flood depth raster, paired with a 512 × 512 DEM and optionally with other spatial layers. In the SGUnet model, the encoder consists of ten 3 × 3 convolutional layers with ReLU activations, distributed across five different feature map resolution levels (two layers at each resolution of 512 × 512, 256 × 256, 128 × 128, 64 × 64, and 32 × 32). The deepest layer of the encoder has 1024 channels, and this represents the most compressed, abstract representation of the input data (known as the bottleneck of the network). Encoder employs 2 × 2 max-pooling four times to down-sample feature maps, reducing their spatial dimensions from 512 × 512 to 32 × 32 and allowing the network to focus on important features.

The right half of the network, known as the decoder (or expanding path), mirrors the encoder, but focuses on upsampling the feature maps to recover spatial information. This part reconstructs the output by increasing the resolution and using convolutions to refine details. The decoder in the SGUnet model consists of eight 3 × 3 convolutional layers with ReLU activations, distributed across four feature map resolution levels (64 × 64, 128 × 128, 256 × 256, and 512 × 512). It employs 2 × 2 transposed convolutions four times to upsample the feature maps from 32 × 32 back to the original resolution of 512 × 512.

U-Net employs skip connections between corresponding layers in the encoder and decoder paths to transfer high-resolution feature maps from the contracting path to the expanding path. In the SGUnet model network, skip connections are used at each level of the decoder to pass high-resolution features from the encoder directly to the decoder. This helps recover spatial details lost during downsampling.

To improve predictive accuracy, SGUnet incorporates attention blocks at critical locations in both encoder and decoder paths, enabling the model to focus on the most relevant spatial features. Attention mechanisms are applied at 256 × 256 and 128 × 128 resolutions in the encoder and at 256 × 256 and 512 × 512 resolutions in the decoder. Each attention block consists of three convolution layers. In the network output layer, a final convolution layer is applied to reduce the number of channels from 64 to 1. Overall, the network consists of 31 convolutional layers and approximately 31 million trainable parameters.

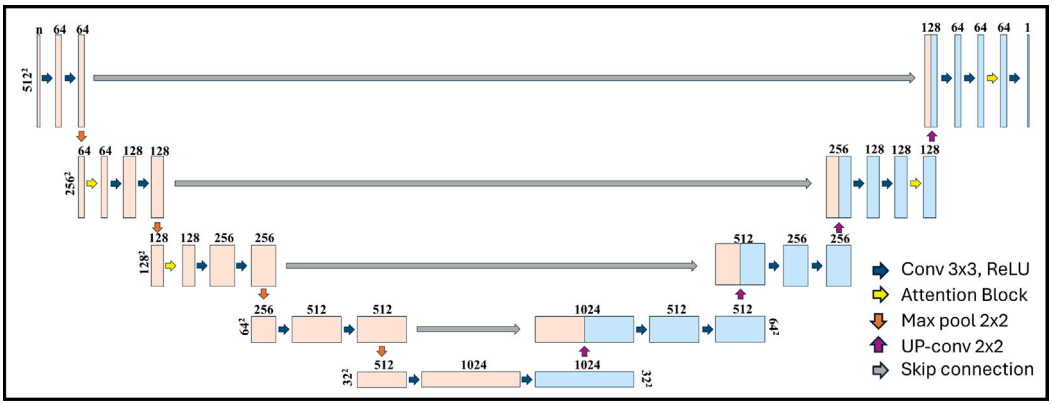

Fig. 2. U-Net-based machine learning architecture of the SGUnet model.

2.1.2. Model training

The SGUnet model is trained using a supervised learning approach to optimize its trainable parameters. The primary input to the SGUnet model is the coarse grid based flood depth images. At the input layer, these images are concatenated with spatial explanatory variables of the study area. In this study, the SGUnet model is tested with single and multiple spatial explanatory variables. When a single variable is used, the DEM images are concatenated with the coarse grid flood depth images, resulting in two input channels. The DEM image is also clipped to match the pixel size of 512 × 512. Each flood depth map, representing different locations and time steps, is combined with the corresponding DEM image along the channel dimension before being passed through the network.

When the SGUnet model is tested with multiple explanatory variables, two additional images, flow accumulation and height above the nearest drainage (HAND) (Nobre et al., 2011), are concatenated with the coarse grid based flood depth images and the DEM images, resulting in a total of four input channels. Flow accumulation quantifies the number of upstream cells flowing into a particular pixel. It indicates the potential for depressions to become inundated, with significantly high accumulation values typically associated with natural watercourses (Löwe et al., 2021). HAND is computed by measuring the vertical distance from each point in a landscape to the nearest drainage or stream. This involves identifying the nearest drainage line for each point and calculating the elevation difference between the point and the drainage. HAND helps to assess how high or low a location is relative to nearby water flow paths, which is crucial for assessing flood potential (Nobre et al., 2011).

Pixel values of all input images, including flood depth maps and spatial explanatory variables, are normalized to a range between 0 and 1 using min–max normalization. For flow accumulation images, an upper cutoff value of 10,000 is applied, and a cube-root transformation is performed before scaling to the [0, 1] range (Löwe et al., 2021). During model training, batches of images are passed through the U-Net to generate predictions. The batch size is determined by the available computational resources, such as GPU memory. The performance of the predictions is evaluated against high-resolution flood depth images using mean squared error (MSE) as the objective function. The SGUnet model uses the Adam optimizer (Kingma and Ba, 2014) to back-propagate the error and adjust the model's weights and biases. Adam optimizer automatically adjusts the learning rate for each parameter, making it effective in handling sparse gradients and noisy data. By incorporating momentum, Adam optimizer accelerates convergence and reduces oscillations (Kapoor et al., 2023). Training continues through multiple epochs until no significant improvement in fitness is observed. After every five epochs, the model is evaluated on a test dataset to detect signs of overfitting, indicated by increasing training fitness while test fitness deteriorates.

2.1.3. Model inference

The overall workflow diagram of the SGUnet model is presented in Fig. 3. The inference process is streamlined as follows.

- *Setup the coarse grid hydrodynamic model:* The coarse grid model can be setup by making the computational grid of the high-resolution fine grid model coarser. Only the computational mesh differs between the two models, while all other parameters, such as boundary conditions, roughness values remain the same.
- *Run the coarse grid hydrodynamic model:* Due to the lower number of computation cells and large computational time steps, the coarse grid model can be run within a few minutes.
- *Load coarse grid hydrodynamic model results into Python environment:* Although, most of the hydrodynamic modeling software facilitate generating flood maps within the modeling software's user interface, the SGUnet model processes raw result files in the Python environment, enhancing computational efficiency and flexibility.
- *Rasterize water surface elevation (WSE) values:* Raw result files store simulations as arrays of WSE values for each computational cell at every time step. At this stage, the geometry of the computational mesh is used to rasterize each WSE value to its corresponding computational cell, aligning it with the resolution of the DEM. Each point in the DEM that falls within a computational cell receives the same WSE value calculated for that cell. This process converts the unstructured WSE values into a structured array that mirrors the dimensions of the DEM.
- *Convert WSE values into water depths:* With each pixel assigned a WSE value from the previous step, water depth values for each DEM point can now be calculated by subtracting the surface elevation from the WSE. Pixels with a positive difference are considered wet or flooded, with water depth values equal to the difference. Conversely, pixels with no difference or a negative difference are labeled as dry, with water depth values set to zero. An example of this process, converting WSE values from mesh resolution to water depth values at DEM resolution, is shown in Fig. 4, where the mesh resolution is 25 m × 25 m, and the DEM resolution is 5 m × 5 m.
- *Thresholding:* To account for numerical errors, a small threshold of 5 cm is applied to distinguish between dry and wet pixels (Löwe et al., 2021). Pixels with water depth values less than 5 cm are considered dry, with their water depth values set to zero.
- *Clip water depth maps:* Given that flood depth maps at DEM resolution may contain millions of pixels, it is impractical to load them as a single image into the ML algorithm. Therefore, the flood maps are clipped into manageable-sized images using a predefined polygon shapefile of square boxes, covering only the flood-prone area of the model domain (hereinafter referred to as clipped area). A pixel size of 512 × 512 is chosen to balance

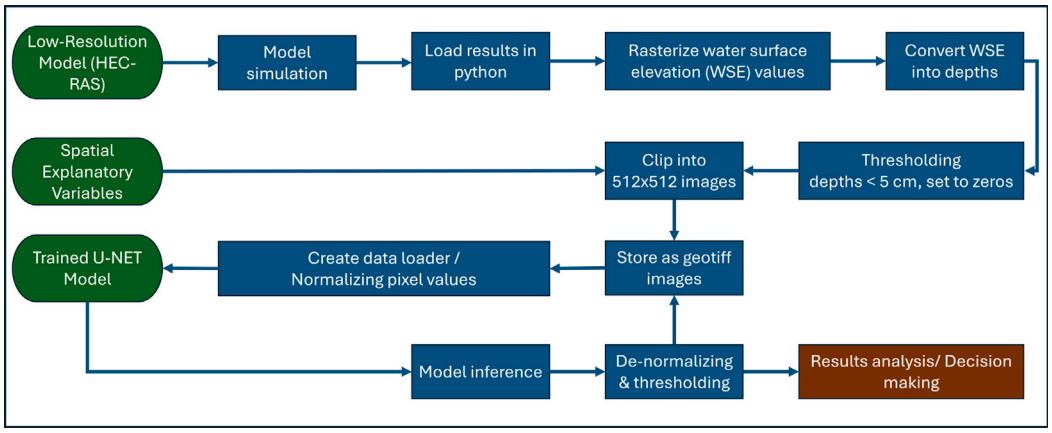

Fig. 3. Workflow diagram of the SGUnet model.

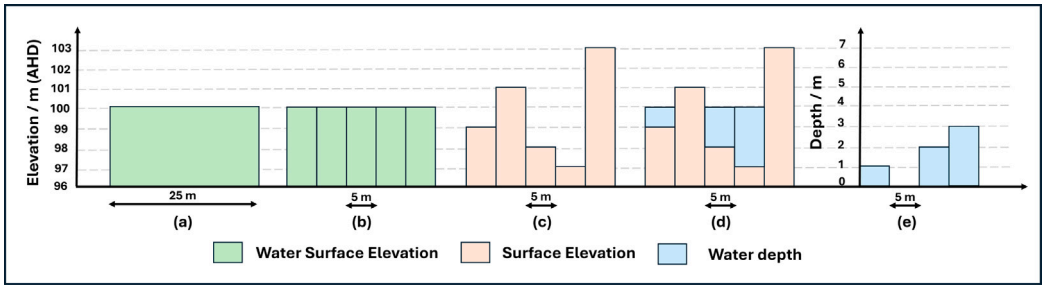

Fig. 4. An example conversion of water surface elevation (WSE) values (above Australian height datum - AHD) into water depth values using subgrid topography. a: WSE value at computational mesh resolution (25 m × 25 m), b: rasterized WSE values at DEM resolution (5 m × 5 m), c: DEM elevations (5 m × 5 m), d: WSE - DEM (5 m × 5 m), e: water depth values at DEM resolution (5 m × 5 m).

computational resources with the physical area captured by each box.

- *Save images:* The water depth maps are saved in the GeoTIFF file format. To reduce file sizes, the water depth arrays are converted to centimeters and saved as integers.
- *Create data loader:* A data loader is created by concatenating coarse grid flood depth images (512 × 512 pixels) with the corresponding spatial explanatory variable images. When a single explanatory variable is used, only the DEM is concatenated with the flood depth images (DEM is also clipped to 512 × 512 images using the same polygon shapefile). When multiple spatial explanatory variables are included, the DEM, flow accumulation, and HAND images are concatenated with the flood depth images. All pixel values are normalized to a range between zero and one.
- *Model inference:* In the final stage, the trained SGUnet model is used to upscale the initial coarse grid flood depth estimates, enhancing their accuracy in a computationally efficient manner. The model's predictions are de-normalized, and the 5 cm threshold is applied again. Users can choose to generate flood depth maps for all time steps across the entire clipped area or focus on a specific area and time interval based on the coarse grid simulation results. The latter option is particularly beneficial for operational flood models, as it provides greater computational efficiency.

2.2. Hydrodynamic modeling

Three large Australian watersheds, namely the Wollombi, Chowilla, and Burnett River, are selected to evaluate the SGUnet model's capability in high-resolution flood mapping. These study areas exhibit distinct flood behaviors in terms of flood type and event duration. For each watershed, both coarse grid and fine grid flood models are established to generate flood depth maps at regular intervals, which are then used for training and testing the SGUnet model. The primary difference between the coarse and fine grid models is the number of computation cells: the fine grid model uses a significantly greater number of cells. However, all other modeling parameters, except for the computation time step (which is larger in the coarse grid model due to its larger cell sizes), remain the same across both models.

In this study, high-resolution fine grid model predictions serve as the target model predictions (i.e., ground truth data). Therefore, a proper calibration with the observed data is not necessary for each flood model. However, to ensure the high-resolution fine grid models' predictions are reliable, simulations were compared with observed data from gauging stations (including both water levels and discharge) during setup. Relevant measured data were obtained from the Bureau of Meteorology, Australia website (Bureau of Meteorology, 2024). Once the high-resolution fine grid model is set up for the catchment of interest, the coarse grid model is generated by simply coarsening the computational mesh. No calibration with observed data was performed for the coarse grid model simulations.

The workflow of the SGUnet model is applicable to any subgrid enabled hydrodynamic modeling software, such as HEC-RAS (US Army Corps of Engineers, 2024b), TUFLOW (BMT Group, 2024), and 3Di (Nelen & Schuurmans, 2024). In this study, the U.S. Army Corps of Engineers' River Analysis System (HEC-RAS) software (version 6.5 for Windows) (US Army Corps of Engineers, 2024a) is utilized to set up both fine and coarse grid flood models for the three study areas. HEC-RAS supports the development of one-dimensional (1D), two-dimensional (2D) and coupled 1D/2D flood models, using both structured grids (with uniform cell spacing) and unstructured grids (with variable cell spacing) (US Army Corps of Engineers, 2024c). Depending on the modeling needs, users can choose between the faster Diffusion Wave Equations (DWE) or the more accurate SWE for 2D unsteady flow routing. For the study areas examined in this research, 2D flood models are set up using unstructured grids. Starting with version 5.0,

HEC-RAS software employs the subgrid technique (Casulli and Stelling, 2011; Casulli, 2009) in flood modeling, which enables a detailed representation of fine-scale topography and flow patterns without the full computational burden of using a highly refined grid. Consequently, the subgrid technique used in HEC-RAS allows for much coarser (and thus faster) coarse grid models in this study.

Sections 2.2.1, 2.2.2, and 2.2.3 provide more details on the flood models developed for the Wollombi, Chowilla, and Burnett Rivers, respectively. Fig. 5 presents the DEMs, while Table 1 summarizes the HEC-RAS model parameters for each catchment.

2.2.1. Wollombi

The Wollombi catchment, located in the Hunter Valley, New South Wales, covers 1870 km^2, and this study focuses on the 814 km^2 downstream subcatchments from Paynes Crossing. Wollombi Creek meets the Hunter River at the catchment outlet. This area is prone to river flooding, with events that typically last only a few days due to the steep topography. More details on the catchment and flood history are available in Singleton Council (2016).

For the high-resolution fine grid HEC-RAS model, three different cell sizes were used, while the coarse grid model employed a uniform cell size. Within the clipped area, the high-resolution fine grid model contained 27.4 times more cells than the coarse grid model. The boundary conditions include one upstream inflow boundary and two downstream water level boundaries. The DWE were deemed sufficient for the Wollombi model, as negligible differences were observed when switching from DWE to SWE.

2.2.2. Chowilla

The Chowilla floodplain, which covers 760 km^2 is another flood-prone riverine area located toward the lower end of the Murray–Darling Basin. The very mild gradient of the topography makes the Chowilla floodplain's flood dynamics to be distinctly different from the other two study areas. Due to its large upstream basin and gentle gradient, flood events in Chowilla can last weeks to months (Fraehr et al., 2023). This area has also been studied in previous research (Fraehr et al., 2024, 2023).

Chowilla flood models have three upstream inflow boundaries and one downstream water level boundary. In the high-resolution fine grid model, two distinct cell sizes were applied, whereas the coarse grid model employed a uniform cell size. Within the clipped area, the high-resolution fine grid model contains 27.7 times more computation cells than the coarse grid model. The DWE proved to be adequate for the Chowilla flood models.

2.2.3. Burnett River

The selected Burnett River study area encompasses the downstream catchment (1197 km^2) from the Paradise Dam, located in the large Burnett Basin (38370 km^2) on the southern Queensland coast, Australia. This region features steep topography, leading to flood events that typically last from several days to weeks due to the fast flow dynamics. The downstream boundary is influenced by tidal effects, making the area prone to compound flooding. Additional details about the study area can be found in Fraehr et al. (2024) and Zhou et al. (2021).

The Burnett River flood models include two upstream inflow boundary conditions and a one-tidal boundary condition downstream. The SWE (full momentum-based equation set) is used to perform flow routing as the DWE is not able to model wave propagation (back water effect) due to tidal influence (US Army Corps of Engineers, 2024c). Both the coarse and fine grid models use uniform cell sizes throughout. Within the clipped area, the high-resolution model contains 86 times more cells than the coarse grid model.

2.3. SGUnet model training

In the current study, the SGUnet model is trained individually for each study area. As described in Section 2.1, after the simulations of the model are generated, flood depth maps are produced at regular intervals. For each study area, the flood-prone regions are identified, and their corresponding flood depth maps are clipped into 512 × 512 pixel images. Fig. 5(d) shows the distribution of clipping boxes for each study area, covering the respective flood-prone areas. The number of training and testing samples varies between study areas due to differences in flood-prone area extents, DEM resolutions (which determine the physical dimensions of the clipping boxes), the number of flood events, their durations, and the intervals at which flood mapping is performed. Additionally, a spin-up period is applied to each flood event during which the flood maps are excluded from the SGUnet model's training and testing datasets.

In this study, model training was conducted on the Gadi platform, part of the supercomputing facility provided by the National Computational Infrastructure (NCI) Australia (NCI Australia, 2024). The Gadi platform operates on the Linux operating system, and the gpuvolta queue, equipped with four Nvidia Tesla Volta V100-SXM2-32 GB GPUs, was used to train the SGUnet model. A batch size of 48 was achievable without exceeding the allocated GPU memory. A low learning rate was necessary for stable model training with 512 × 512 pixel-sized images. Specific details regarding model training are summarized in Table 2.

2.4. Performance evaluation

The upskilling capability of the proposed SGUnet model is assessed in terms of both flood depth prediction accuracy and flood extent (inundation) prediction accuracy. Both SGUnet model and coarse grid model predictions are compared against the high-resolution fine grid model predictions.

2.4.1. Flood depth

Pixel to pixel water depth predictions between the target image (high-resolution fine grid model predictions) and predicted image (either coarse grid model or SGUnet model predictions) are evaluated using the root mean squared error (RMSE). RMSE is calculated for each flood mapping time step during the test events using the Eq. (1) while an average RMSE value for an event is calculated using the Eq. (2). Similarly, an average mean absolute error per event is derived using the Eq. (3).

$$\mathrm{RMSE_t} = \sqrt{\frac{1}{N}\sum_{i=1}^{N}\left(y_{it} - \hat{y}_{it}\right)^2} \tag{1}$$

$$\mathrm{AvgRMSE} = \sqrt{\frac{1}{T}\frac{1}{N}\sum_{t=1}^{T}\sum_{i=1}^{N}\left(y_{it} - \hat{y}_{it}\right)^2} \tag{2}$$

$$\mathrm{AvgMAE} = \frac{1}{T}\frac{1}{N}\sum_{t=1}^{T}\sum_{i=1}^{N}\left|y_{it} - \hat{y}_{it}\right| \tag{3}$$

where y_{it} and $\hat{y}_{it}$ are the water depths at pixel i at time t of the target image and the predicted image, respectively. T is the total number of flood mapping time steps during the event and N is the total number of pixels in each water depth map.

For visual comparison, water depth difference maps and scatter plots are generated, comparing predicted values against the target values. In this analysis, two key flood maps are used: the peak flood depth map and the maximum flood depth map. The peak flood depth map represents flood depths when the total flood volume across the entire model domain reaches its maximum at a specific time during the event. In contrast, the maximum flood depth map shows the highest flood depth reached by each pixel during the event, with different pixels potentially reaching their maximum depths at different times.

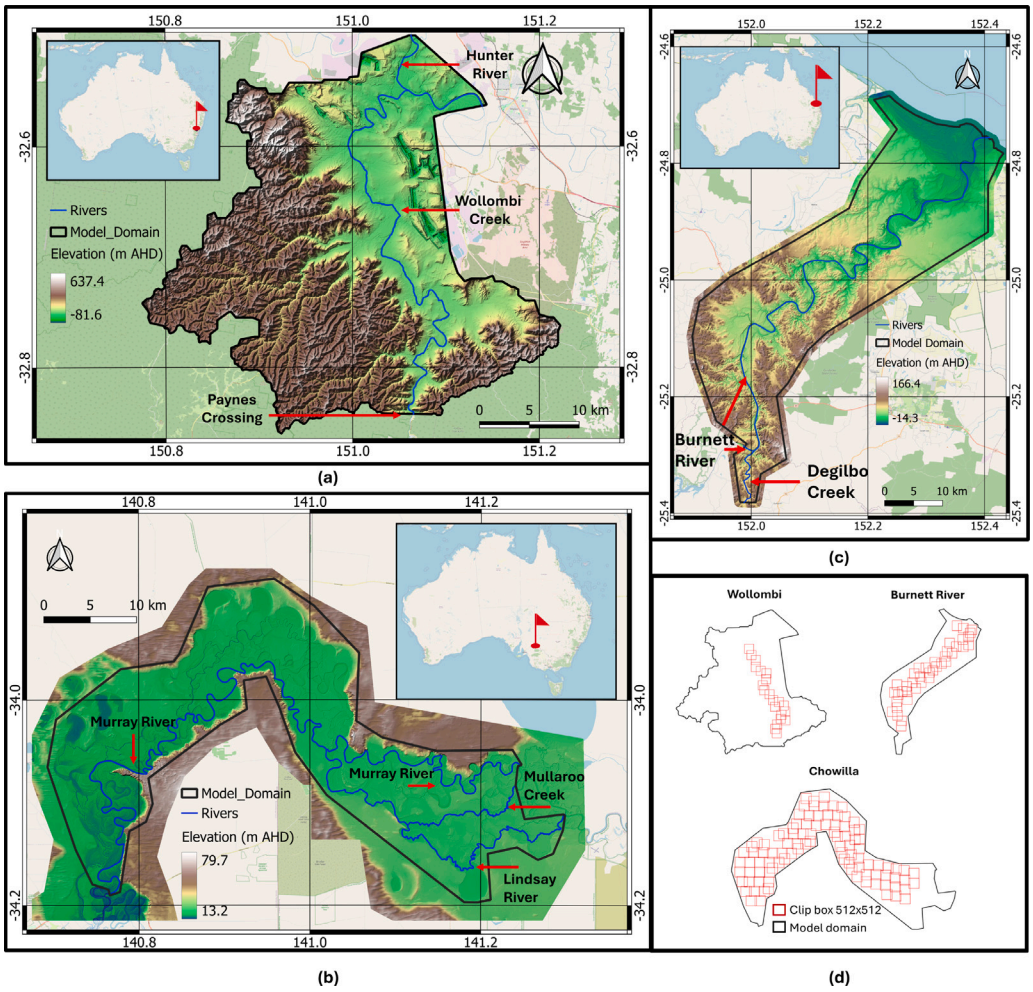

Fig. 5. Digital elevation models of (a) Wollombi, (b) Chowilla, (c) Burnett River, and (d) clip boxes distribution of each catchment.

2.4.2. Flood extent

Flood extents or inundation maps are binary representations of flood depth maps and are crucial for allocating flood mitigation resources during a flood event (Fraehr et al., 2024). In these maps, pixels with water depth values above a certain threshold are marked as flooded cells (value = 1), while pixels below this threshold are marked as dry cells (value = 0). After converting flood maps (maps generated from coarse grid model, high-resolution fine grid model and SGUnet model) into inundation maps, three metrics are calculated: probability of detection (POD), rate of false alarms (RFA), and critical success index (CSI) (Schaefer, 1990).

POD (Eq. (4)) reflects the model's ability to detect true positives (pixels correctly identified as flooded). A POD of 1 indicates a perfect detection (i.e., all flooded pixels in the high-resolution flood map are captured by the prediction model). RFA (Eq. (5)) measures the portion of predicted floods that did not actually occur. The optimum RFA value is zero where there are no false alarms. POD and RFA should be interpreted together. For example, a model predicting everywhere flooded has a perfect POD value but with a high RFA value. Therefore, a model with a high POD and a low RFA is considered as a good prediction model.

CSI (Eq. (6)) measures the overall accuracy of the model in predicting inundation extents by considering both false alarms and misses. It combines aspects of POD and RFA, making it a commonly used metric for evaluating flood inundation models. CSI ranges from 0 to 1, with 1 indicating perfect forecasts. It balances between the sensitivity of the model (POD) and its tendency to give false alarms (RFA).

$$\text{Probability of detection (POD)} = \frac{TP}{TP + FN} \tag{4}$$

$$\text{Rate of false alarms (RFA)} = \frac{FP}{TP + FP} \tag{5}$$

$$\text{Critical success index (CSI)} = \frac{TP}{TP + FN + FP} \tag{6}$$

Where true positives (TP) refer to the number of pixels that are marked as flooded in both the predicted image and the target image. False positives (FP) are the number of pixels that are marked as flooded in the predicted image, but are dry in the target image. False negatives (FN) indicate the number of pixels that are marked as dry in the predicted image but are flooded in the target image.

3. Results and discussion

3.1. Single vs multiple spatial explanatory variables

For the three study areas, first, the SGUnet model is trained with both single (coarse grid flood depth image + DEM) and multiple (coarse grid flood depth image + DEM + HAND + flow accumulation) spatial explanatory variables. The goal of this exercise was to determine whether incorporating additional hydrological knowledge explicitly (through multiple spatial explanatory variables) would offer any benefit. Both HAND and flow accumulation images were derived from the DEM of each study area. For each catchment, all training parameters were kept constant except for the number of input channels, and the model was trained for a specified number of epochs: 75 epochs for Wollombi, 15 epochs for Chowilla, and 50 epochs for Burnett River.

Table 1
Parameter details of the HEC-RAS models (BC: boundary condition, stn no: station number).

Parameter	Wollombi	Chowilla	Burnett River
Model area (km^2)	814	760	1197
Model type	2D	2D	2D
DEM resolution (m)	5 × 5	5 × 5	10 × 10
DEM source	Commonwealth of Australia (Geoscience Australia) (2021)	Fraehr (2023)	Commonwealth of Australia (Geoscience Australia) (2021)
No of cells: Domain			
Coarse grid	21,715	4622	8704
Fine grid	204,862	130,621	488,080
No of cells: Clipped area			
Coarse grid	2612	3421	4601
Fine grid	71,487	94,780	395,792
Cell size: Fine grid			
Near streams (m)	25 × 25	25 × 25	40 × 40
Floodplain (m)	40 × 40	100 × 100	40 × 40
Other (m)	200 × 200	100 × 100	40 × 40
Cell size: Coarse grid			
Entire domain (m)	200 × 200	400 × 400	400 × 400
Average cell size (m^2)			
Coarse grid	40,397	164,320	162,574
Fine grid	4282	5814	2899
Break line usage	used only in fine grid models for all three catchments		
Equation set	DWE	DWE	SWE
Rain on grid	Yes	No	No
Rainfall interpolation	IDW	–	–
Roughness	spatially varying based on land use for all three catchments		
Inflow BC: stn no	210135 (Bureau of Meteorology, 2024)	426200, 414211, 414212 (Fraehr, 2023)	136007A, 136011A (Bureau of Meteorology, 2024)
Downstream BC: stn no	210127, 210134 (Bureau of Meteorology, 2024)	A4260512 (Fraehr, 2023)	Bundaberg (Maritime Safety Queensland, 2024)
Evaporation	No	No	No
Infiltration	No	No	No
No of events	4	6	4
Event duration	several days	weeks to months	days to weeks
Mapping interval (hours)	0.5	6.0	0.5
Computation time step	controlled based on the Courant number		

Table 2
SGUnet model training details of the three case studies.

Parameter	Wollombi	Chowilla	Burnett River
No of clip boxes (512 × 512)	21	100	40
Clip box size (km)	2.56	2.56	5.12
Clipped area (km^2)	95.3	513.2	684.2
Spin-up period (days)	1	12	1
No of samples (train/test)	35280/6048	160200/49400	83520/15360
No of epochs	75	15	200
Batch size	48	48	48
Learning rate	0.00002	0.00002	0.00002

Table 3
Mean squared error (MSE) values from training and testing of models with single and multiple spatial explanatory variables.

Parameter	Wollombi	Chowilla	Burnett River
No of epochs	after 75	after 15	after 50
Training MSE (cm^2)			
Single spatial explanatory variable	13.44	7.51	490.30
Multiple spatial explanatory variables	12.84	7.97	500.22
Testing MSE (cm^2)			
Single spatial explanatory variable	17.02	7.16	770.54
Multiple spatial explanatory variables	17.75	6.58	788.14

Following the training phase, the models were evaluated using the testing data.

Fig. 6 displays the training loss curves for each study area, illustrating the variation in training MSE values throughout the training epochs. Additionally, Table 3 presents the final MSE values for both the training and testing phases, comparing models that utilized single and multiple spatial explanatory variables. Incorporating more input images significantly increased the training time; the SGUnet model with multiple spatial explanatory variables required 20% more training time compared to the single-variable case. However, as shown in Fig. 6, adding more explanatory variables did not yield any notable improvement in terms of training or testing accuracy, nor in the convergence speed.

Thus, it would be safe to assume that, when the SGUnet model is trained for each catchment individually, incorporating more explicit hydrological information adds little or no advantage. However, it is important to highlight that only hydrological information derived from the DEM was used in this experiment. The deep network layers of the SGUnet model may be capable of extracting this information from the DEM alone when used as the sole spatial explanatory variable. Therefore, all subsequent results in this paper are based on using the DEM as the only spatial explanatory variable.

It was also observed that most fitness improvements occurred within the first few epochs of training, indicating that the SGUnet model can quickly learn the underlying upscaling patterns with minimal training effort.

3.2. Water depths

The top three graphs in Fig. 7, show the RMSE of the coarse grid model's depth predictions and the SGUnet model's depth predictions

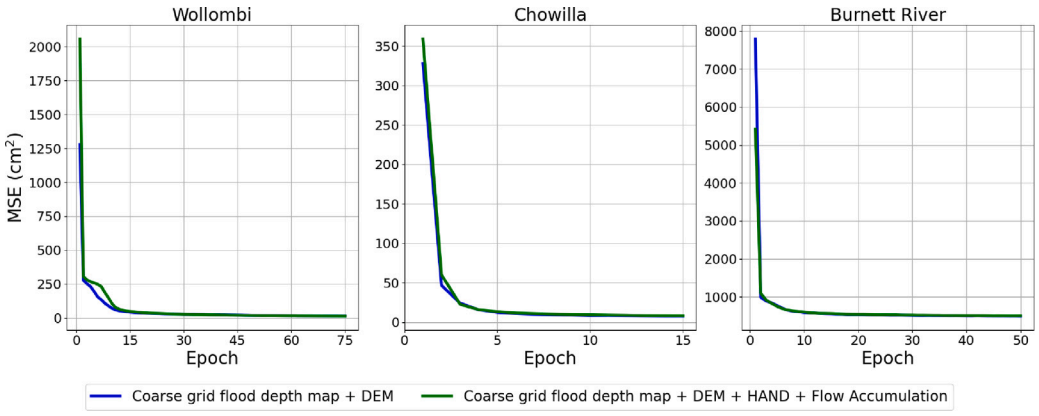

Fig. 6. Training period mean squared error (MSE) values: single vs. multiple spatial explanatory variables.

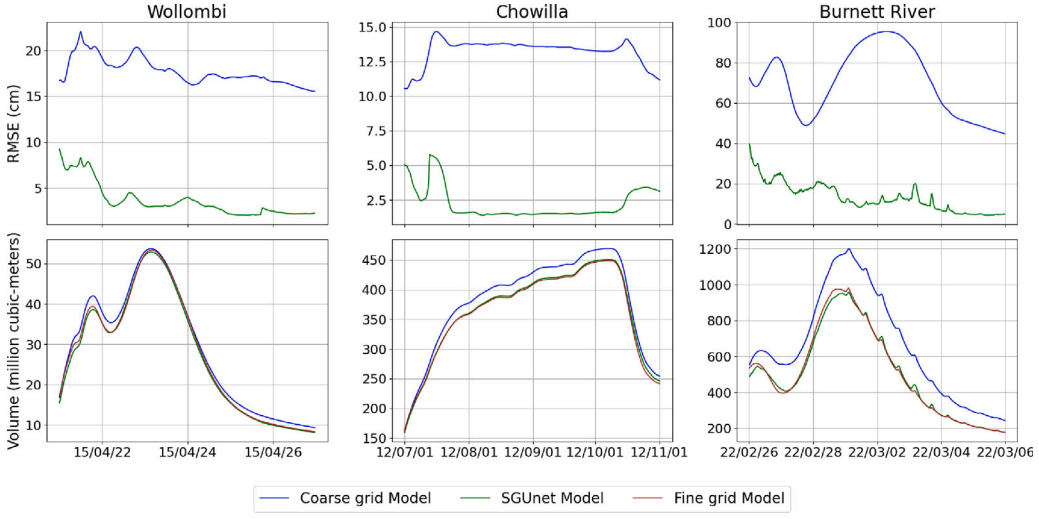

Fig. 7. Root mean square error (RMSE) and flood volume for each time step during testing events of Wollombi, Chowilla, and Burnett River.

compared to the high-resolution fine grid model's depth predictions at each time step of the testing events for the three study areas. The three bottom plots represent the flood volume distribution of the high-resolution fine grid, coarse grid, and SGUnet models during the testing event for each model domain. The averaged RMSE and MAE values for the coarse grid and SGUnet models during the testing periods are provided in Table 4. Here, for each model, at each time step, a flood depth map is created for the clipped area by merging the depth predictions of each clip box (average value is used for overlapping pixels).

As shown in Fig. 7, for each study area and at each time step of the testing event, the RMSE between the water depth estimates of the SGUnet model and those of the high-resolution fine grid model (green line) is significantly lower than the RMSE between the estimates of the coarse grid based model and the estimates of the high-resolution fine grid model (blue line). Among the coarse-grid models, the smallest discrepancy with the flood depths of the high-resolution fine-grid model is observed in the Chowilla floodplain, while the largest discrepancy is seen in the Burnett River basin.

The Burnett River basin is the most complex hydrodynamic model of the three domains, due to its steep terrain and the backwater effect from tidal influence. Therefore, when the cell sizes are coarsened, the depth estimates tend to deviate more from the target values. Additionally, the difference in the number of computation cells between the coarse-grid and high-resolution fine-grid models is greatest for the Burnett River basin, further explaining why the coarse-grid depth estimates differ significantly from the high-resolution fine-grid model estimates compared to the other two cases.

The Chowilla floodplain has the simplest hydrological model configuration. The difference in the number of computation cells between the coarse and fine grid models is also smaller compared to that of the Burnett River basin, similar to the Wollombi models. Due to flat terrain, increasing the computation cell sizes causes smaller variations in depth estimates compared to steep terrain. This explains why the difference in flood estimates between the coarse and fine grid models is relatively smaller for the Chowilla floodplain.

In terms of complexity, the Wollombi flood dynamics fall between the Chowilla and Burnett River models. As expected, the difference in flood depth estimates between the coarse and fine grid models for Wollombi lies between those of the other two cases. This pattern is also reflected in the number of epochs required for SGUnet model training, with the Burnett River requiring the most (200 epochs), the Chowilla floodplain the least (15 epochs), and Wollombi falling in between (75 epochs).

The ratio of the averaged RMSE between the coarse grid model and the SGUnet model for Wollombi, Chowilla, and Burnett River is 4.5, 5.3, and 4.9, respectively. So, regardless of the model complexities and computation mesh differences between coarse and fine grid models, the trained SGUnet model for each domain has achieved a similar level of improvement in flood depth estimates.

A general trend is noticeable in the flood volume plots. At each occasion, coarse grid model (blue line) over predicts the actual flooding. This may be due to the prediction of more flooded areas and

Table 4
Performance metrics for water depth and inundation predictions.

Metric	Wollombi		Chowilla		Burnett River	
	Low-res	SGUnet	Low-res	SGUnet	Low-res	SGUnet
AvgRMSE (cm)	17.8	4.0	13.3	2.5	72.1	14.8
AvgMAE (cm)	5.5	1.1	7.7	1.0	24.5	3.7
POD_{5cm}	0.837	0.910	0.985	0.990	0.969	0.969
POD_{30cm}	0.900	0.961	0.980	0.995	0.971	0.965
RFA_{5cm}	0.118	0.035	0.068	0.010	0.165	0.034
RFA_{30cm}	0.107	0.011	0.078	0.007	0.173	0.022
CSI_{5cm}	0.753	0.881	0.918	0.981	0.814	0.937
CSI_{30cm}	0.812	0.950	0.905	0.988	0.807	0.945

high flood depths. However, more importantly, the SGUnet model significantly reduces this volume error in all three cases, as the green line closely follows the brown line (representing the high-resolution fine-grid model).

The SGUnet model's ability to improve coarse grid based simulated flood depth estimates can be visually observed in the absolute flood depth difference maps shown in Fig. 8. For each study area, the absolute flood depth differences are plotted between the coarse grid and high-resolution fine-grid model estimates (left side) and the SGUnet and high-resolution fine grid model estimates (right side). These maps are generated for both peak flood depth (blue outlines) and maximum flood depth (red outlines) in each domain, using the same depth scale across all maps of the same catchment for easy comparison.

As clearly shown, once the SGUnet model is applied, the predictions become much closer to those of the high-resolution fine grid model, with the differences approaching zero. This behavior is consistent for both peak flood depth maps and maximum flood depth maps. As noted with RMSE values, the largest discrepancies in flood depth estimates are observed in the Burnett River, while the smallest occur in the Chowilla floodplain.

In the Burnett River flood maps, the improvement in flood depth prediction is more pronounced in the upstream areas compared to the regions near the tidal boundary. However, even with coarse grid model, the flood depth differences are smaller close to the tidal boundary as hydrodynamic models force cells in the vicinity of the boundary to respond to the boundary signal (known as the effect of the boundary conditions). Additionally, in some localized areas, the SGUnet model does not perform as well as in other regions. This could potentially be improved by adjusting the coarse grid model configuration in those specific areas, such as adding a refinement zone.

Fig. 9 presents scatter plots that compare flood depth predictions from the high-resolution fine grid model with those from the coarse grid model (blue dots) and the SGUnet model (green dots). The left-hand side shows plots for peak depth maps, while the right-hand side displays plots for maximum depth maps. It is evident that the SGUnet model's flood depth estimates, in both peak and maximum flood maps, are much closer to the high-resolution fine grid model's values. This is illustrated by the green dots clustering closer to the 45-degree line (red dotted line) in each model domain.

Accurately distinguishing between overestimation and underestimation in model predictions relative to target values is crucial in any flood study. Fig. 10 illustrates five categories of flood depth differences identified for each catchment by comparing the coarse-grid model and SGUnet model against fine-grid model simulations (target values). The flood depth difference is computed by subtracting model predictions from the target values, where negative differences indicate overestimation and positive differences indicate underestimation. The identified categories are as follows: differences less than −30 cm are classified as overestimated, between −5 cm and −30 cm as slightly overestimated, between −5 cm and 5 cm as matched, between 5 cm and 30 cm as slightly underestimated, and greater than 30 cm as underestimated. We consider differences within the range of −30 cm to 30 cm as the comparable zone with the target values, since vertical accuracies of DEMs range within this limits.

As shown in the depth difference histograms in Fig. 10 for each catchment, the SGUnet model effectively corrects both the overestimated and underestimated regions of the coarse grid model, shifting them into the comparable zone. The coarse-grid model simulations for the Wollombi catchment exhibit a significant number of overestimated and underestimated regions (pixels). In contrast, the SGUnet model significantly reduces the underestimated regions and eliminates the overestimated regions. The percentage of matched areas in the SGUnet model is 17.8% higher than that of the coarse grid model.

For the Chowilla catchment, most of the coarse grid model simulations already fall within the comparable zone. However, the SGUnet model further refines these predictions, shifting them almost entirely into the matched category (98.8% compared to 50% in the coarse grid model). This highlights how the upskilling process benefits from more accurate coarse grid estimates.

In contrast, the coarse-grid model simulations for the Burnett River basin show the largest deviation from the fine-grid model simulations, with a significant overestimation of flood depth values. However, the SGUnet model effectively reduces this overestimation, shifting most of the overestimated regions into the comparable zone (with the overestimated area decreasing from 23.4% in the coarse grid model to just 2.2% in the SGUnet model). Notably, while the SGUnet model introduces a slight underestimation in 0.4% of the area, the coarse grid model had no underestimated regions.

Neither DEM correction steps, such as DEM smoothing or sink filling, nor local refinements of the coarse grid model mesh based on upscaling results were applied. However, since the accuracy of the initial coarse-grid estimates significantly influences the upscaling performance of the SGUnet model, incorporating such approaches may further enhance its capabilities. Therefore, exploring these refinements in future research would be worthwhile.

3.3. Inundation

Fig. 11 illustrates three metrics used to evaluate the flood extent prediction capability of the SGUnet model (green lines) during the testing events of each case study. For comparison, the same metrics are calculated for the coarse grid model predictions (blue lines). A low threshold of 5 cm (dotted lines) and a high threshold of 30 cm (solid lines) are used separately to identify dry and wet cells. Table 4 summarizes the average metric values for both the coarse grid and SGUnet models with these two thresholds. Generally, the performance of each metric for both models improves as the flood detection threshold increases. With the only exception of POD_{30cm} value for the Burnett River (difference is only 0.006), the SGUnet model performs better than the coarse grid model in flood inundation predictions across all metrics.

As noted previously, coarse grid models tend to overpredict flooding in terms of both area and depth. In doing so, coarse-grid models capture most of the true flooding areas as well. Hence, coarse-grid models also have higher POD values. However, except in some instances in the Burnett River basin, the SGUnet model achieves even higher POD values than the coarse grid models. This suggests that the SGUnet model is better at identifying true flooding areas that the coarse grid models may miss.

As shown in the RFA plots (middle three plots of Fig. 11), coarse grid models typically exhibit a high rate of false alarms. This issue is where coarse grid models lose most of their prediction accuracy compared to high-resolution fine grid models in flood extent prediction. Consequently, it is crucial for the SGUnet model to significantly reduce RFA values during the upskilling process. Notably, for each study domain, the SGUnet models effectively reduce the RFA values to levels closer to zero at each time step of the testing events.

However, the CSI value provides a more comprehensive measure of overall inundation prediction capability, as it combines both POD

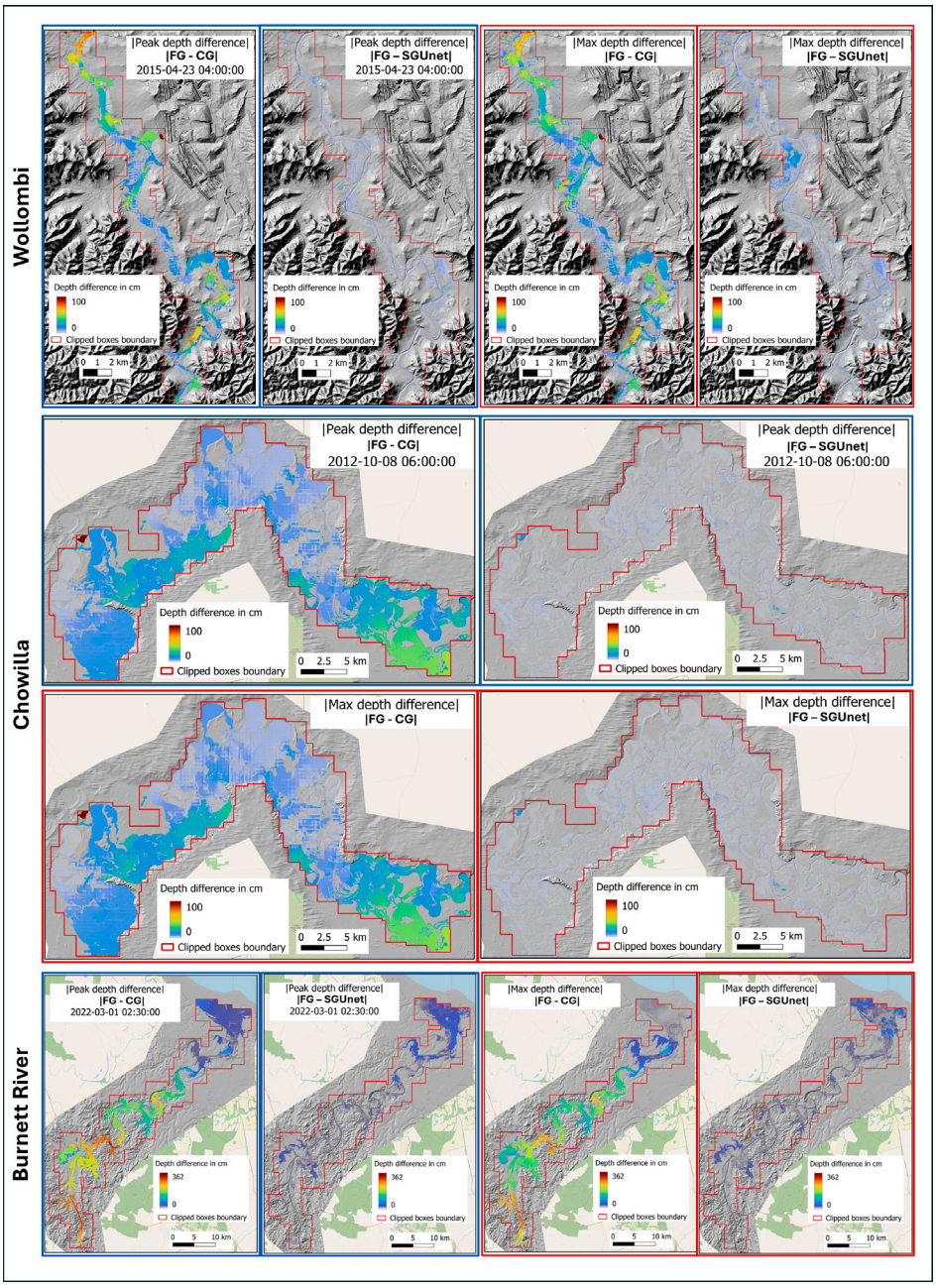

Fig. 8. Absolute water depth differences in peak and max flood depth maps between fine grid model & coarse grid model ($|FG - CG|$), and between fine grid model & SGUnet model ($|FG - SGUnet|$).

and RFA values. As illustrated in the CSI plots (bottom three plots of Fig. 11), the SGUnet models consistently achieve considerably higher CSI values than the coarse grid models for all three watersheds at each time step. This clearly highlights the superior flood inundation mapping capability of the SGUnet model, with CSI values exceeding 0.9 for most of the event duration.

3.4. Computational efficiency

The speed-up ratios achieved by the trained SGUnet models vary across the three case studies due to differences in the configurations of the fine and coarse grid models, the duration of the test event, and the number of clip boxes used. It is true that a pure ML based surrogate model might achieve a higher speed-up ratio compared to the SGUnet model. This is because, by being a hybrid model, SGUnet model requires the initial flood depth estimates from a coarse grid flood model. Thus, there is an upper bound for the speed-up ratio that the model can achieve.

For example, in the Wollombi case study, the coarse grid model took 5 min and 12 s to complete the simulation on an average computer (Intel i5 1.90 GHz processor, 16 GB RAM, 12 solver cores), while the high-resolution fine grid model required 7 h, 46 min, and 18 s. The pre-processing steps of the SGUnet model, which convert raw HEC-RAS model results from the coarse grid model into input samples for the learning algorithm, took 2 min and 53 s. The SGUnet model inference was completed in 1 min and 12 s, with the SGUnet model running on the NCI Gadi platform (details provided in Section 2.3). Thus, the SGUnet model achieves a speed-up ratio of approximately 50 for the Wollombi case study.

This speed-up ratio does not include the time required to setup and train the SGUnet model, which is a one-time task performed before the model can be used repeatedly in an operational setting. For the

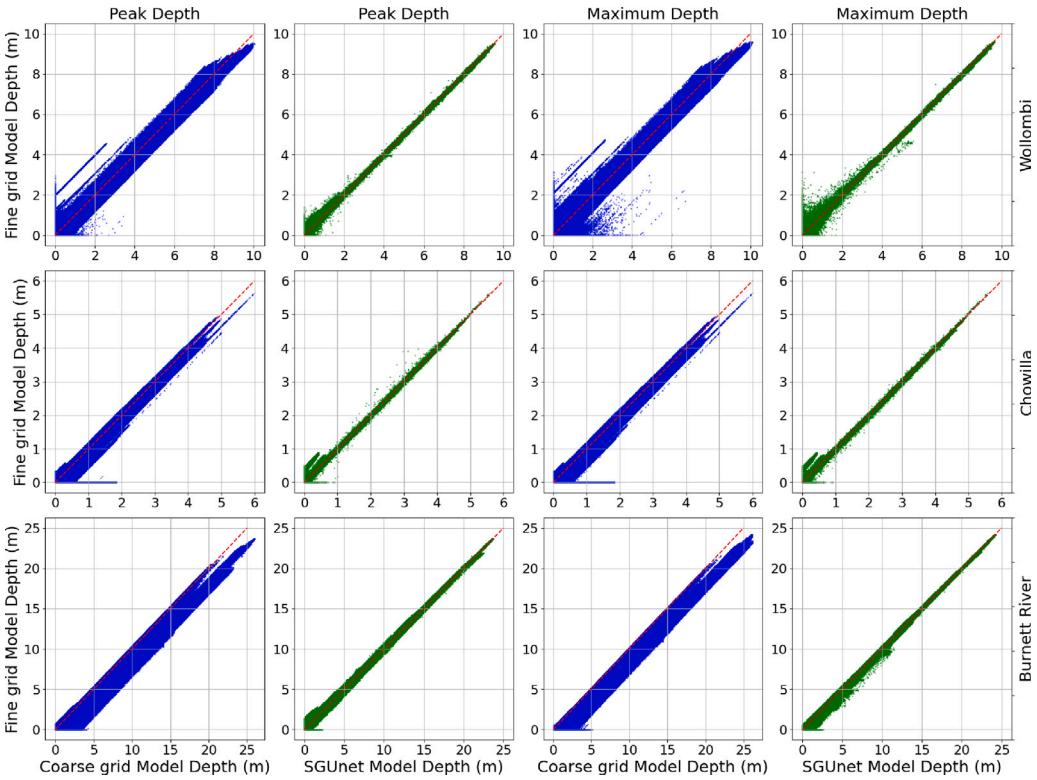

Fig. 9. Water depth scatter plots of peak flood and max flood maps between coarse grid model & fine grid model, and between SGUnet model & fine grid model.

Wollombi model, training with 35,280 input samples and a batch size of 48 over 75 epochs took 13 h and 25 min. However, the model converged to a value close to its final fitness within the first few epochs, indicating that most of the progress was made early in the training process.

While model inference is critical in an operational flood model, development time is also important for the model's practicality and scalability. Reducing development time allows for faster deployment, continuous updates, and easier adaptation to new regions or changing environmental conditions. As a result, future research on SGUnet will focus on developing a more generalized model that can be applied to different flood-prone areas with minimal additional training, rather than building a new model from scratch for each region. Developing a more generalized model with pretrained weights would reduce the training effort needed when applying SGUnet to new domains.

The timing details mentioned above encompass the generation of all flood depth maps for the clipped area throughout the test event, totaling 6048 images (21 clip boxes and 288 time steps). However, since the SGUnet model uses coarse grid model estimates at a specific time step to generate high-resolution fine grid predictions for the same time step, it is possible to apply the SGUnet model to generate flood maps for a specific local area within the clipped region and for a particular time period within the event. This approach could yield even higher speed-up ratios, making it more suitable for operational flood modeling.

3.5. LSG model vs SGUnet model

The LSG model (Fraehr et al., 2023) is an advanced hybrid flood modeling framework that integrates a low-fidelity hydrodynamic model with ML to predict both flood extent and water depth. It leverages Empirical Orthogonal Functions analysis to reduce the dimensionality of spatial–temporal flood data and employs Sparse Gaussian Process models to map low-fidelity simulations to high-fidelity outputs. By efficiently upscaling coarse grid flood predictions to fine grid resolution, the LSG model achieves high prediction accuracy while maintaining computational efficiency.

More importantly, a recent benchmark study (Fraehr et al., 2024) demonstrated that the LSG model outperformed four other state-of-the-art ML-based surrogate models in predicting flood extent and depth across multiple basins, including the Burnett River basin used in this study. Consequently, the LSG model is trained using Burnett River catchment data, and its flood depth and extent predictions are compared against those of the SGUnet model. Since the LSG model produces water level predictions at the fine grid mesh resolution, these are converted to DEM-resolution water depths using subgrid topography to enable a direct comparison with the SGUnet model.

The average RMSE for the test event, relative to the simulations of the fine grid model, is 72.1 cm for the coarse grid model, 17.0 cm for the LSG model and 14.8 cm for the SGUnet model. During the critical six-hour period near the peak flood depth, the average RMSE increases to 82.6 cm for the coarse grid model and slightly decreases to 16.9 cm for the LSG model and drops to 11.4 cm for the SGUnet model. Both the LSG and SGUnet models significantly improve flood depth predictions of the coarse grid model, with SGUnet achieving the highest accuracy. Notably, SGUnet considerably outperforms LSG near the peak flood depth, the most critical period in flood modeling. Fig. 12 (left) illustrates the variation in RMSE during this six-hour window, showing that SGUnet maintains consistent performance, while the LSG model exhibits greater variability.

A similar pattern is observed in the accuracy of the prediction of flood extent between the two models. Fig. 12 (right) illustrates the CSI variation during the six-hour window. Across both threshold values, the SGUnet model achieves higher CSI values than the LSG model and exhibits less variability. In contrast, the LSG model reaches its lowest CSI value at peak flood depth but improves as it moves away from the peak. The average CSI values over the entire event for the LSG and SGUnet models are both 0.937 with a 5 cm threshold, and 0.940 and 0.945, respectively, with a 30 cm threshold. During the critical six-hour window, these values increase to 0.952 and 0.967 (5 cm

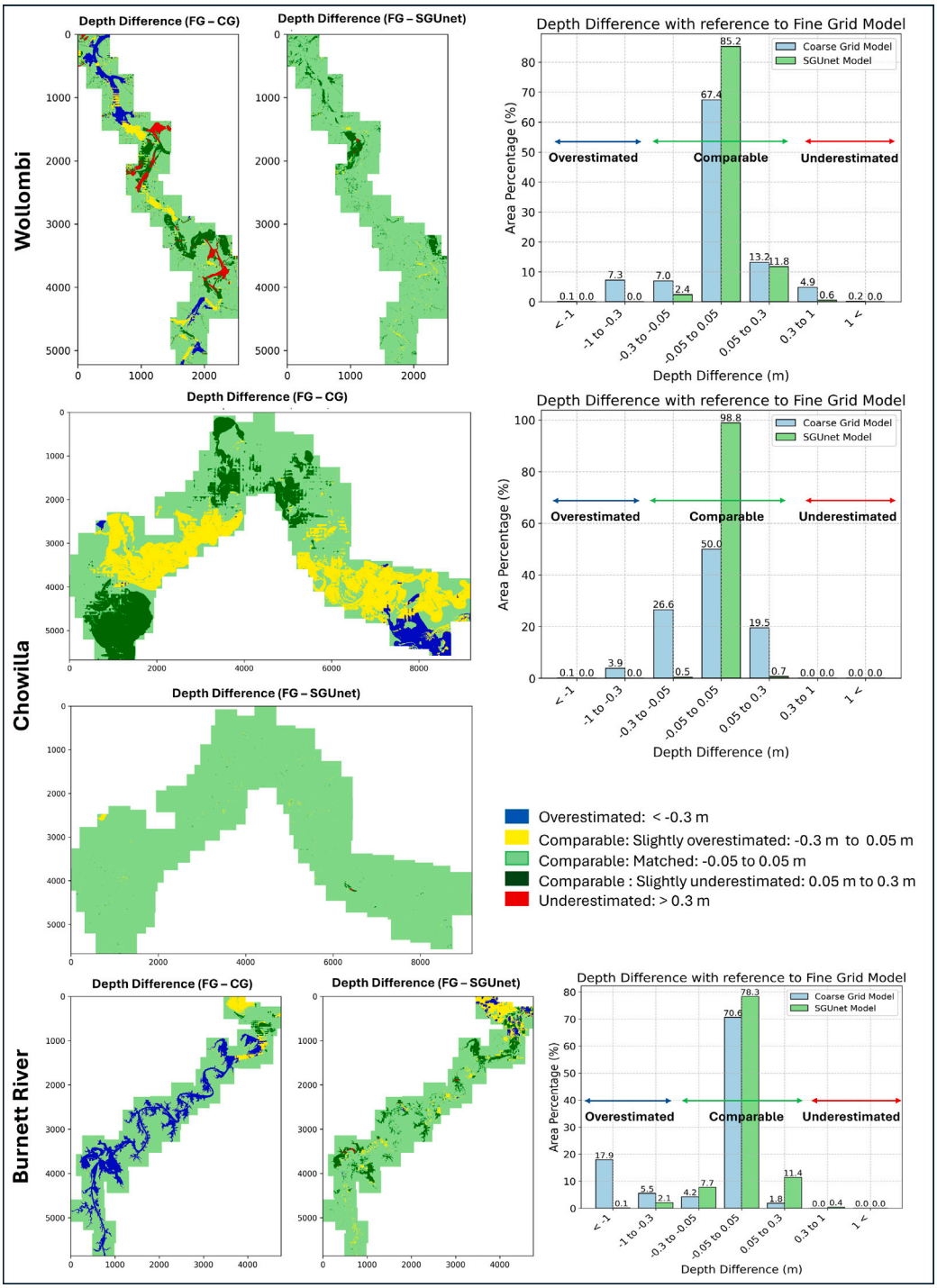

Fig. 10. Water depth difference categories of max flood depth maps between fine grid model & coarse grid model (FG - CG), and between fine grid model & SGUnet model (FG - SGUnet).

threshold) and 0.949 and 0.971 (30 cm threshold). However, compared to the coarse grid model (event-averaged CSI and six-hour window CSI of 0.814 and 0.807 for the 5 cm threshold, and 0.842 and 0.839 for the 30 cm threshold), both the LSG and SGUnet models provide significantly improved flood extent predictions.

Although the SGUnet model achieves higher accuracy in both flood depth and extent predictions for the Burnett River basin, it is equally important to compare the model development and inference times of the two models. A direct timing comparison is not provided here, as the models were executed on different hardware platforms—LSG on a multi-CPU system and SGUnet on a multi-GPU system.

Model development time includes both data preparation and ML training. Although the LSG model requires significantly less training time, achieving the same accuracy as SGUnet may require several additional training events, necessitating multiple fine-grid model runs. As a result, the overall data preparation time for LSG is higher, making the total development effort for both models comparable.

In terms of inference, the SGUnet model directly outputs predictions at DEM resolution, whereas the LSG model produces results at fine-grid mesh resolution. Because LSG predicts at a significantly lower number of points than SGUnet, its inference speed is higher. However, SGUnet does not require post-processing, while LSG necessitates an additional

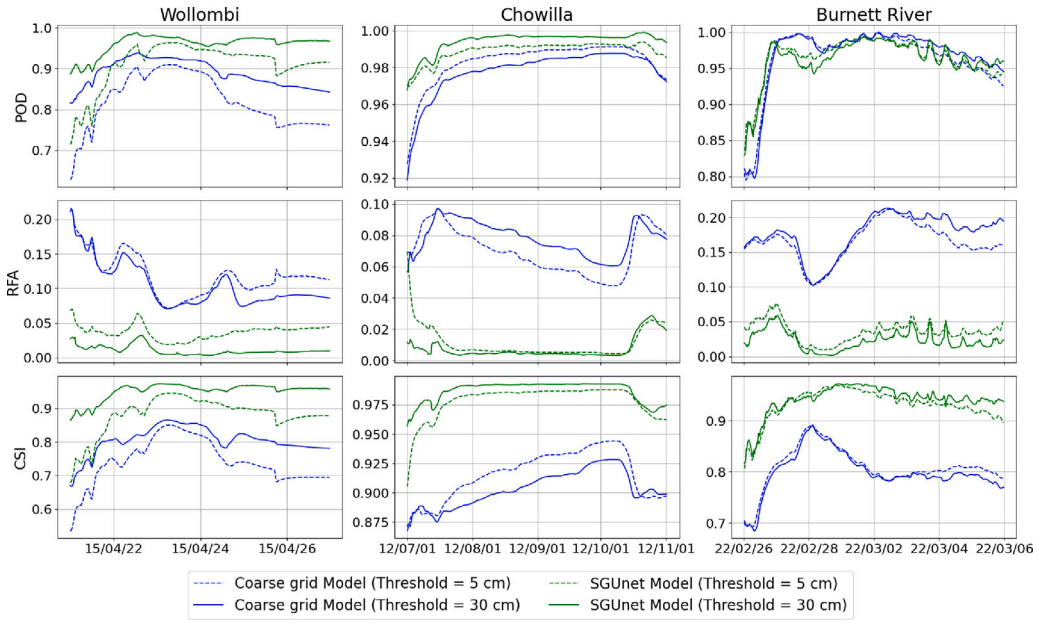

Fig. 11. Probability of detection (POD), rate of false alarm (RFA), and critical success index (CSI) for each time step during testing events of Wollombi, Chowilla, and Burnett River.

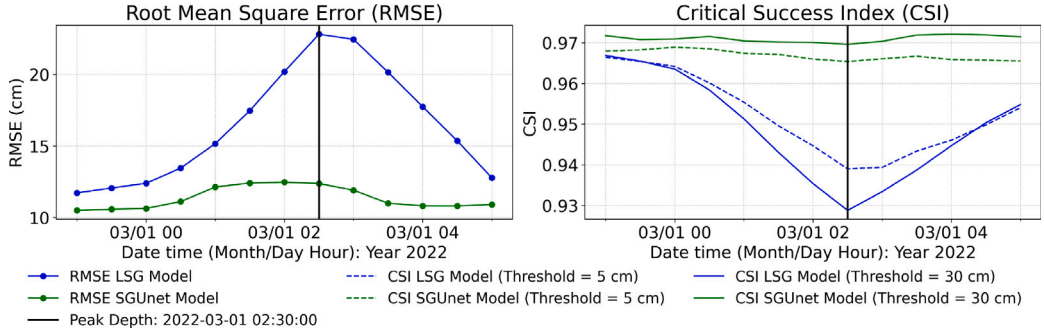

Fig. 12. Comparison of root mean square error (RMSE) and critical success index (CSI) between the LSG model and SGUnet model near the peak flood for the Burnett River.

step to map predictions to DEM resolution, which offsets some of its inference speed advantage. Consequently, the total inference times of both models are comparable.

3.6. Role of subgrid based coarse grid initial estimates

Subgrid-based coarse grid models, such as HEC-RAS in this study, can produce results that are highly correlated with high-resolution fine-grid models. This makes them valuable as initial estimates to guide learning algorithms while maintaining computational efficiency, a key principle underlying the development of SGUnet.

SGUnet is a hybrid upscaling framework for coarse grid, subgrid-based flood models. The subgrid technique is a purely numerical upscaling method that generates high-resolution flood maps at the underlying terrain resolution, independent of the computational grid resolution. However, when coarse-grid flood models generate flood depth maps at DEM resolution, they often introduce incorrect flooding patterns compared to maps created by high-resolution fine-grid models due to limitations of momentum descriptions at coarse grid levels. Hence, the primary role of the SGUnet model is to correct the predictions in the flood depth maps by the coarse grid model.

Importantly, the subgrid modeling approach used in the coarse-grid hydrodynamic model simplifies the ML-based upscaling process. This is because the coarse grid model already incorporates high-resolution terrain data for flood routing calculations, and the terrain data is used again during the conversion from water level elevations at computational grid resolution to water depths at DEM resolution. This simplification is evident in the early convergence observed with each SGUnet model trained in this study. Furthermore, each model was able to learn the upscaling patterns using a relatively small number of flood events.

Although a purely ML-based surrogate model might offer greater computational efficiency than the SGUnet hybrid model, the latter provides more reliable predictions. This is because SGUnet starts with robust initial estimates based on physics, making it easier to understand the predictions of the model compared to the opaque nature of pure ML models. Additionally, the SGUnet model requires less training compared to a pure ML model, benefiting from good initial guesses.

In this study, coarse grid models were created by coarsening the computational grid of the high-resolution fine grid model without fine-tuning or calibrating against observed data. In operational settings, a one-time setup could include some rough calibration or fine-tuning of the coarse grid model, which would further improve the performance of the SGUnet model in high-resolution flood mapping. Since the performance of the coarse grid model significantly influences both accuracy and computational efficiency, these adjustments could lead to even better results.

4. Conclusions

High-resolution fine-grid hydrodynamic models are computationally expensive and often require hours or days to complete simulations. In contrast, coarse-grid models can deliver results in minutes, but at the cost of reduced accuracy. SGUnet addresses this trade-off by leveraging physics-based coarse-grid hydrodynamic simulations as initial estimates and refining them using a U-Net-based upscaling model. The improved accuracy of the SGUnet model stems from the subgrid approach and supervised learning approach, where a U-Net architecture is trained to correct coarse grid model predictions at subgrid levels, where subgrid resolution is the same as the DEM, by learning their relationship with fine grid model outputs, also at DEM resolution.

SGUnet significantly enhances flood depth and extent predictions, reducing RMSE by a factor of 4.5–5.3 compared to coarse-grid models, achieving a CSI values above 0.9 for flood extent mapping, and delivering a 50× speed-up over fine-grid hydrodynamic models. It also outperforms the state-of-the-art ML-based upscaling model, LSG. Unlike purely data-driven approaches, SGUnet benefits from physics-based initial estimates, improving reliability and interpretability.

Tested in multiple study areas, SGUnet demonstrated robust performance in learning upscaling patterns, even with limited training data. The use of subgrid hydrodynamic models simplifies data preprocessing, allowing for efficient and early convergence. Although the current implementation conditions SGUnet on DEM data, future versions could incorporate additional spatial variables to further enhance generalizability.

SGUnet model is just a beginning of applying super-resolution networks to upscale coarse-grid flood depth simulations for rapid high-resolution flood mapping. Using a U-Net architecture with attention mechanisms, it effectively reconstructs high-resolution flood maps from sparse hydrodynamic simulations. Future research will focus on extending SGUnet's spatial and temporal extrapolation capabilities, benchmarking it against other surrogate models, and integrating advanced generative artificial intelligence techniques such as diffusion models.

CRediT authorship contribution statement

Herath Mudiyanselage Viraj Vidura Herath: Writing – review & editing, Writing – original draft, Visualization, Validation, Software, Resources, Methodology, Investigation, Formal analysis, Data curation, Conceptualization. **Lucy Marshall:** Writing – review & editing, Visualization, Supervision, Resources, Methodology, Investigation, Conceptualization. **Abhishek Saha:** Writing – review & editing, Visualization, Validation, Software, Methodology, Conceptualization. **Sanka Rasnayaka:** Writing – review & editing, Software, Methodology, Conceptualization. **Sachith Seneviratne:** Writing – review & editing, Software, Methodology, Conceptualization.

Declaration of Generative AI and AI-assisted technologies in the writing process

During the preparation of this work the authors used ChatGPT in order to improve the readability and language of the manuscript. After using this tool, the authors reviewed and edited the content as needed and take full responsibility for the content of the published article.

Declaration of competing interest

The authors declare that they have no known competing financial interests or personal relationships that could have appeared to influence the work reported in this paper.

Data availability

Data will be made available on request.

References

Begmohammadi, A., Wirasaet, D., Silver, Z., Bolster, D., Kennedy, A.B., Dietrich, J., 2021. Subgrid surface connectivity for storm surge modeling. Adv. Water Resour. 153, 103939. http://dx.doi.org/10.1016/j.advwatres.2021.103939, URL https://linkinghub.elsevier.com/retrieve/pii/S0309170821000944.

Bentivoglio, R., Isufi, E., Jonkman, S.N., Taormina, R., 2022. Deep learning methods for flood mapping: a review of existing applications and future research directions. Hydrol. Earth Syst. Sci. 26 (16), 4345–4378. http://dx.doi.org/10.5194/hess-26-4345-2022, URL https://hess.copernicus.org/articles/26/4345/2022/.

BMT Group, 2024. TUFLOW: Hydrodynamic modelling software. https://www.tuflow.com. Version 2024.01, accessed: 2024-09-04.

Bryant, S., Schumann, G., Apel, H., Kreibich, H., Merz, B., 2024. Technical Note: Resolution enhancement of flood inundation grids. Hydrol. Earth Syst. Sci. 28 (3), 575–588. http://dx.doi.org/10.5194/hess-28-575-2024, URL https://hess.copernicus.org/articles/28/575/2024/.

Bureau of Meteorology, 2024. Water data online. http://www.bom.gov.au/waterdata/, accessed: 2024-09-04.

Buwalda, F.J.L., De Goede, E., Knepflé, M., Vuik, C., 2023. Comparison of an explicit and implicit time integration method on GPUs for shallow water flows on structured grids. Water 15 (6), http://dx.doi.org/10.3390/w15061165, URL https://www.mdpi.com/2073-4441/15/6/1165.

Carreau, J., Guinot, V., 2021. A PCA spatial pattern based artificial neural network downscaling model for urban flood hazard assessment. Adv. Water Resour. 147, 103821. http://dx.doi.org/10.1016/j.advwatres.2020.103821, URL https://www.sciencedirect.com/science/article/pii/S0309170820307107.

Casulli, V., 2009. A high-resolution wetting and drying algorithm for free-surface hydrodynamics. Internat. J. Numer. Methods Fluids 60 (4), 391–408. http://dx.doi.org/10.1002/fld.1896.

Casulli, V., 2019. Computational grid, subgrid, and pixels. Internat. J. Numer. Methods Fluids 90 (3), 140–155. http://dx.doi.org/10.1002/fld.4715, URL https://onlinelibrary.wiley.com/doi/10.1002/fld.4715.

Casulli, V., Stelling, G.S., 2011. Semi-implicit subgrid modelling of three-dimensional free-surface flows. Internat. J. Numer. Methods Fluids 67, 441–449. http://dx.doi.org/10.1002/fld.2361, URL https://onlinelibrary.wiley.com/doi/10.1002/fld.2361.

Chadalawada, J., Herath, H.M.V.V., Babovic, V., 2020. Hydrologically informed machine learning for rainfall-runoff modeling: A genetic programming-based toolkit for automatic model induction. Water Resour. Res. 56 (4), http://dx.doi.org/10.1029/2019wr026933.

Commonwealth of Australia (Geoscience Australia), 2021. Elvis - elevation and depth - foundation spatial data. https://elevation.fsdf.org.au/, accessed: 2024-09-04.

Darvishi, S., 2025. Monitoring and modeling vulnerability of land use changes in the current flood hazard conditions using novel hybrid GIS-based approaches and remote sensing data. Earth Sci. Informatics 18, 189. http://dx.doi.org/10.1007/s12145-024-01643-6.

El baida, M., Boushaba, F., Chourak, M., et al., 2024. Real-time urban flood depth mapping: Convolutional neural networks for pluvial and fluvial flood emulation. Water Resour. Manag. 38, 4763–4782. http://dx.doi.org/10.1007/s11269-024-03886-w.

Fraehr, N., 2023. Data from HEC-RAS models for training and validation in "Development of a fast and accurate hybrid model for floodplain inundation simulations" (Version 2) [Dataset]. The University of Melbourne, http://dx.doi.org/10.26188/21235782.

Fraehr, N., Wang, Q.J., Wu, W., Nathan, R., 2023. Development of a fast and accurate hybrid model for floodplain inundation simulations. ESSOAr v1, http://dx.doi.org/10.22541/essoar.168563136.64954780/v1.

Fraehr, N., Wang, Q.J., Wu, W., Nathan, R., 2024. Assessment of surrogate models for flood inundation: The physics-guided LSG model vs. state-of-the-art machine learning models. Water Res. 252, 121202. http://dx.doi.org/10.1016/j.watres.2024.121202.

He, J., Zhang, L., Xiao, T., Wang, H., Luo, H., 2023. Deep learning enables super-resolution hydrodynamic flooding process modeling under spatiotemporally varying rainstorms. Water Res. 239, 120057. http://dx.doi.org/10.1016/j.watres.2023.120057, URL https://linkinghub.elsevier.com/retrieve/pii/S0043135423004931.

Herath, H.M.V.V., Chadalawada, J., Babovic, V., 2021a. Genetic programming for hydrological applications: to model or to forecast that is the question. J. Hydroinformatics 23 (4), 740–763. http://dx.doi.org/10.2166/hydro.2021.179, URL https://iwaponline.com/jh/article/23/4/740/81446/Genetic-programming-for-hydrological-applications.

Herath, H.M.V.V., Chadalawada, J., Babovic, V., 2021b. Hydrologically informed machine learning for rainfall–runoff modelling: towards distributed modelling. Hydrol. Earth Syst. Sci. 25 (8), 4373–4401. http://dx.doi.org/10.5194/hess-25-4373-2021, URL https://hess.copernicus.org/articles/25/4373/2021/.

Jamali, A., Roy, S.K., Hashemi Beni, L., Pradhan, B., Li, J., Ghamisi, P., 2024. Residual wave vision U-Net for flood mapping using dual polarization Sentinel-1 SAR imagery. Int. J. Appl. Earth Obs. Geoinf. 127, 103662. http://dx.doi.org/10.1016/j.jag.2024.103662, URL https://www.sciencedirect.com/science/article/pii/S1569843224000165.

Kapoor, A., Pathiraja, S., Marshall, L., Chandra, R., 2023. DeepGR4J: A deep learning hybridization approach for conceptual rainfall-runoff modelling. Environ. Model. Softw. 169, 105831. http://dx.doi.org/10.1016/j.envsoft.2023.105831, URL https://www.sciencedirect.com/science/article/pii/S1364815223002177.

Karpatne, A., Atluri, G., Faghmous, J.H., Steinbach, M., Banerjee, A., Ganguly, A., Shekhar, S., Samatova, N., Kumar, V., 2017. Theory-guided data science: A new paradigm for scientific discovery from data. IEEE Trans. Knowl. Data Eng. 29 (10), 2318–2331. http://dx.doi.org/10.1109/TKDE.2017.2720168.

Kennedy, A.B., Wirasaet, D., Begmohammadi, A., Sherman, T., Bolster, D., Dietrich, J., 2019. Subgrid theory for storm surge modeling. Ocean. Model. 144, 101491. http://dx.doi.org/10.1016/j.ocemod.2019.101491, URL https://linkinghub.elsevier.com/retrieve/pii/S1463500319301155.

Kingma, D.P., Ba, J., 2014. Adam: A method for stochastic optimization. arXiv preprint arXiv:1412.6980.

Li, J., Huang, H., He, W., Zhang, H., Zhang, L., 2024. Overcoming the uncertainty challenges in flood rapid mapping with multi-source optical data. In: IGARSS 2024 - 2024 IEEE International Geoscience and Remote Sensing Symposium. pp. 780–784. http://dx.doi.org/10.1109/IGARSS53475.2024.10641074.

Löwe, R., Böhm, J., Jensen, D.G., Leandro, J., Rasmussen, S.H., 2021. U-FLOOD – Topographic deep learning for predicting urban pluvial flood water depth. J. Hydrol. 603, 126898. http://dx.doi.org/10.1016/j.jhydrol.2021.126898.

Madake, J., Mali, R., Shahapure, A., More, P., Bhatlawande, S., 2024. FloodDetectionNet: U-net attention Based Flooded Area segmentation. In: Ragavendiran, S.D.P., Pavaloaia, V.D., Mekala, M.S., Cabezuelo, A.S. (Eds.), Innovations and Advances in Cognitive Systems. Springer Nature Switzerland, Cham, pp. 319–333.

Maritime Safety Queensland, 2024. Open data. URL https://www.msq.qld.gov.au/tides/open-data, accessed: 2024-09-04.

NCI Australia, 2024. Supercomputing. URL https://nci.org.au/our-services/supercomputing, accessed: 2024-09-04.

Nelen & Schuurmans, 2024. 3Di: Flexible hydrodynamic modelling suite. https://www.3diwatermanagement.com. Version 2.2.1, accessed: 2024-09-04.

Nobre, A.D., Cuartas, L.A., Hodnett, M., Rennó, C.D., Rodrigues, G., Silveira, A., Waterloo, M., Saleska, S., 2011. Height above the nearest drainage – a hydrologically relevant new terrain model. J. Hydrol. 404 (1–2), 13–29. http://dx.doi.org/10.1016/j.jhydrol.2011.03.051.

Paszke, A., Gross, S., Massa, F., Lerer, A., Bradbury, J., Chanan, G., Killeen, T., Lin, Z., Gimelshein, N., Antiga, L., Desmaison, A., Kopf, A., Yang, E., DeVito, Z., Raison, M., Tejani, A., Chilamkurthy, S., Steiner, B., Fang, L., Bai, J., Chintala, S., 2019. PyTorch: An imperative style, high-performance deep learning library. Advances in Neural Information Processing Systems 32 (NeurIPS 2019). https://pytorch.org/.

Python Software Foundation, 2024. Python language reference, version 3.x. https://www.python.org/, accessed: 2024-09-07.

Rak, A., Mewis, P., Guthe, S., 2024. Accelerating flash flood simulations: An efficient GPU implementation for a slim shallow water solver. Environ. Model. Softw. 177, 106030. http://dx.doi.org/10.1016/j.envsoft.2024.106030, URL https://www.sciencedirect.com/science/article/pii/S1364815224000914.

Ranasinghe, N., Xia, Y., Seneviratne, S., Halgamuge, S., 2024. GINN-KAN: Interpretability pipelining with applications in physics informed neural networks. arXiv:2408.14780.

Ronneberger, O., Fischer, P., Brox, T., 2015. U-net: Convolutional networks for biomedical image segmentation. In: Medical Image Computing and Computer-Assisted Intervention–MICCAI 2015. Springer International Publishing, Lima, Peru, pp. 234–241. http://dx.doi.org/10.48550/arXiv.1505.04597.

Schaefer, J.T., 1990. The critical success index as an indicator of warning skill. Weather. Forecast. 5 (4), 570–575. http://dx.doi.org/10.1175/1520-0434(1990)005<0570:TCSIAA>2.0.CO;2.

Shao, Y., Chen, J., Zhang, T., Yu, T., Chu, S., 2024. Advancing rapid urban flood prediction: a spatiotemporal deep learning approach with uneven rainfall and attention mechanism. J. Hydroinformatics 26 (6), 1409–1424. http://dx.doi.org/10.2166/hydro.2024.024, URL https://iwaponline.com/jh/article/26/6/1409/102466/Advancing-rapid-urban-flood-prediction-a.

Singleton Council, 2016. Wollombi brook flood study - report. https://flooddata.ses.nsw.gov.au/related-dataset/wollombi-brook-flood-study-report, accessed: 2024-09-04.

Solaimani, K., Darvishi, S., Shokrian, F., 2024. Assessment of machine learning algorithms and new hybrid multi-criteria analysis for flood hazard and mapping. Environ. Sci. Pollut. Res. 31, 32950–32971. http://dx.doi.org/10.1007/s11356-024-33288-9.

Solaimani, K., Shokrian, F., Darvishi, S., 2023. An assessment of the integrated multi-criteria and new models efficiency in watershed flood mapping. Water Resour. Manag. 37, 403–425. http://dx.doi.org/10.1007/s11269-022-03380-1.

Stelling, G.S., 2022. Boosted robustness of semi-implicit subgrid methods for shallow water flash floods in hills. Comput. & Fluids 247, 105645. http://dx.doi.org/10.1016/j.compfluid.2022.105645, URL https://www.sciencedirect.com/science/article/pii/S0045793022002419.

The Insurance Council of Australia, 2024. Catastrophe 221: NSW and south east queensland floods. https://insurancecouncil.com.au/news-hub/current-catastrophes/catastrophe-221-storms-in-south-east-qld-and-northern-nsw/, accessed: 2024-09-11.

Thisanke, H., Deshan, C., Chamith, K., Seneviratne, S., Vidanaarachchi, R., Herath, D., 2023. Semantic segmentation using Vision Transformers: A survey. Eng. Appl. Artif. Intell. 126, 106669. http://dx.doi.org/10.1016/j.engappai.2023.106669, URL https://www.sciencedirect.com/science/article/pii/S0952197623008539.

Tuyen, D.N., Tuan, T.M., Son, L.H., Ngan, T.T., Giang, N.L., Thong, P.H., Hieu, V.V., Gerogiannis, V.C., Tzimos, D., Kanavos, A., 2021. A novel approach combining particle swarm optimization and deep learning for flash flood detection from satellite images. Mathematics 9 (22), http://dx.doi.org/10.3390/math9222846, URL https://www.mdpi.com/2227-7390/9/22/2846.

US Army Corps of Engineers, 2024a. HEC-RAS downloads. URL https://www.hec.usace.army.mil/software/hec-ras/download.aspx, accessed: 2024-09-04.

US Army Corps of Engineers, 2024b. HEC-ras: River analysis system. https://www.hec.usace.army.mil/software/hec-ras/. Version 6.5, accessed: 2024-09-04.

US Army Corps of Engineers, 2024c. HEC-ras user's manual. URL https://www.hec.usace.army.mil/confluence/rasdocs/rasum/latest, accessed: 2024-09-04.

World Health Organisation, 2024. Floods. https://www.who.int/health-topics/floods#tab=tab_1, accessed: 2024-09-11.

Ye, Z., Shi, F., Zhao, X., Hu, Z., Malej, M., 2021. A data-driven approach to modeling subgrid-scale shallow marsh hydrodynamics. Coast. Eng. 166, 103856. http://dx.doi.org/10.1016/j.coastaleng.2021.103856, URL https://linkinghub.elsevier.com/retrieve/pii/S037838392100017X.

Yin, Z., Saadati, Y., Hu, B., Leon, A.S., Amini, M.H., McDaniel, D., 2024. Fast high-fidelity flood inundation map generation by super-resolution techniques. J. Hydroinformatics 26 (1), 319–336. http://dx.doi.org/10.2166/hydro.2024.228, URL https://iwaponline.com/jh/article/26/1/319/99791/Fast-high-fidelity-flood-inundation-map-generation.

Zhou, Y., Wu, W., Nathan, R., Wang, Q.J., 2021. A rapid flood inundation modelling framework using Deep Learning with spatial reduction and reconstruction. Environ. Model. Softw. 143, 105112. http://dx.doi.org/10.1016/j.envsoft.2021.105112.

Zuhairi, A.H., Yakub, F., Zaki, S.A., Ali, M.S.M., 2022. Review of flood prediction hybrid machine learning models using datasets. IOP Conf. Ser.: Earth Environ. Sci. 1091 (1), 012040. http://dx.doi.org/10.1088/1755-1315/1091/1/012040.